



Recent advances in developing natural and impurity-induced small/no-ELM H-mode regimes in EAST

G. S. Xu¹ · Y. F. Wang¹ · Q. Q. Yang¹ · X. Lin¹ · R. Chen¹ · Y. Ye² · H. Lan^{1,3,4} · N. Yan¹

Received: 18 May 2022 / Accepted: 12 February 2023 / Published online: 1 March 2023
© The Author(s) 2023

Abstract

One critical issue in steady-state and high-performance operation in future tokamak fusion reactors is to develop H-mode operational regimes that mitigate or eliminate the large-amplitude ELMs to decrease the transient heat flux on the divertor and first wall. This paper reviews recent advances in extending and understanding the access and sustainment of natural and impurity-induced small/no-ELM H-mode regimes in EAST. Highly reproducible stationary grassy ELM regime with good energy confinement and excellent tungsten impurity exhaust capability has been obtained in EAST with water-cooled metal wall, compatible with low rotation, high normalized density, high bootstrap current fraction, radiative divertor and fully non-inductive operations, which are the conditions required for future fusion reactor-level plasmas. Grassy-like small-ELM H-mode regime has been achieved in helium (He) plasma experiments, which will be conducted during the pre-fusion power operation phase in ITER. The exploration for type-II ELM regime in EAST is also briefly introduced. Three spontaneous no-ELM H-mode regimes frequently observed in EAST are introduced, including an enhanced-recycling no-ELM regime, a non-inductive low-recycling no-ELM regime and a transient spontaneous no-ELM regime at relatively low pedestal collisionality ($\nu_e^* < 1$). These no-ELM regimes show different characteristic signatures of pedestal fluctuation and profiles, and the physical mechanisms behind have been studied. In addition, small/no-ELM regimes with impurity seeding have also been achieved in EAST. The ELM behavior changing from mixed small and large ELMs to pure grassy ELMs has been observed with neon (Ne) seeding. A highly reproducible no-ELM H-mode regime with radiative divertor has been demonstrated through CD₄ seeding in EAST. These results are believed to be helpful for the application of small/no-ELM H-mode regimes to future tokamak fusion reactors.

Keywords Edge localized modes (ELMs) · Pedestal · Impurity seeding · Radiative divertor · EAST tokamak

Extended author information available on the last page of the article

1 Introduction

Tokamak fusion reactors, like the International Thermonuclear Experimental Reactor (ITER) (Shimada et al. 2004) and the Chinese Fusion Engineering Test Reactor (CFETR) (Wan et al. 2017), are designed based on the high-confinement mode (H-mode), since the machine size and cost are reduced with increasing energy confinement. The high confinement performance results from a transport barrier spontaneously formed at the plasma edge region, called pedestal. However, H-mode plasmas are usually accompanied by a quasi-periodic edge magnetohydrodynamic (MHD) instability, i.e. edge localized modes (ELMs). Large-amplitude ELMs, so-called type-I or giant ELMs, can release large amounts of particles and energy in each burst, resulting in severe damage to the plasma facing components in future tokamak fusion reactors and thus significantly reducing their lifetime (Loarte et al. 2003a; Zhitlukhin et al. 2007; Roth et al. 2009; Klimov et al. 2009; Ueda et al. 2017; Ibano et al. 2019). The impurities generated during ELM bursts can also contaminate the bulk plasma and degrade the plasma confinement. Furthermore, large ELMs can trigger even dangerous global MHD instabilities or collapses of internal transport barriers (ITB). It is therefore currently one of the major threats to the tokamak steady-state operations and thus a high-priority issue in the magnetic fusion research.

To mitigate or eliminate the large ELMs, while at the same time, maintain the high plasma confinement performance, various small/no-ELM H-mode regimes have been developed on present tokamak devices (Viezza 2018; Labit et al. 2019; Harrer et al. 2022; Garcia et al. 2022). The Experimental Advanced Superconducting Tokamak (EAST) (Wan, et al. 2006) aims to provide supports for future tokamak fusion reactors in both physics and technology issues on high confinement and long-pulse operations. Lots of works have been done in EAST to develop H-mode operational regimes that mitigate or eliminate the large amplitude ELMs and meanwhile maintain the high confinement performance, including the natural small/no-ELM regimes (Xu et al. 2019; Yang et al. 2020; Feng et al. 2019; Wang et al. 2014; Ye et al. 2017; Ye et al. 2019; Zhang et al. 2019) and the small/no-ELM regimes obtained with active ELM control techniques (Sun et al. 2016; Sun et al. 2021; Liang et al. 2013; Xu 2020; Zou et al. 2012; Hu et al. 2015; Mansfield et al. 2013). The former refers to intrinsic small/no-ELMs obtained without active ELM control methods, such as the grassy-ELM regime (Xu et al. 2019; Yang et al. 2020), I-mode (Feng et al. 2019) and several spontaneous no-ELM H-mode regimes (Wang et al. 2014; Ye et al. 2017; Ye et al. 2019; Zhang et al. 2019). The latter refers to small/no-ELMs obtained with external active ELM control methods, such as the externally applied magnetic perturbations (Sun et al. 2016), lower hybrid wave (LHW) (Liang et al. 2013), impurity seeding (Xu 2020; Sun et al. 2021), supersonic molecular beam injection (SMBI) (Zou, et al. 2012), real-time lithium (Li) aerosol injection (Hu et al. 2015) and Li granule (Mansfield et al. 2013). The physical mechanisms behind these small/no-ELM regimes are still unclear although the access conditions for achieving these regimes are known. Robust control of large-amplitude ELMs in future fusion reactors still awaits a deeper understanding of the ELM instability.

It has been widely recognized that it is the peeling–ballooning mode (PBM) that mainly limits the pedestal stability, which is coupled by the ballooning mode and kink/peeling mode at a high edge pressure gradient and a high edge current density (Connor et al. 1998; Wilson et al. 1999), providing the trigger for large-amplitude type-I ELMs. Besides the PBMs, some local modes (Wang et al. 2014; Ye et al. 2017; Dunne et al. 2017; Dickinson et al. 2014; Bokshi et al. 2016; Wolfrum et al. 2017) have also been found to affect the pedestal in a very narrow region, which would drive pedestal transport and change the pedestal structure and ELM instability. In recent advances in developing small/no-ELM regimes, it has been found that the density pedestal profile plays an important role in several tokamaks, such as the grassy ELM regime achieved with the RMP-induced pedestal density pump-out in DIII-D (Nazikian et al. 2018), the natural grassy ELM regimes achieved with a low-density pedestal gradient and a high $n_{e,sep}/n_{e,ped}$ in both DIII-D (Wang et al. 2021) and EAST (Xu et al. 2019), the small ELM regimes with a high separatrix density in AUG (Harrer et al. 2018) and TCV (Labit et al. 2019), the ELM-free H-mode regimes obtained with lithium powder injection or lithium-wall coating in DIII-D (Osborne et al. 2015) and NSTX (Maingi et al. 2009) and the low-recycling no-ELM H-mode regime characterized by a low separatrix density in EAST (Ye et al. 2019).

In this paper, a review of recent advances in developing natural and impurity-induced small/no-ELM H-mode regimes in EAST is presented. This paper is organized as follows: Sect. 2 presents recent progress in the small ELM regimes. The progress in extending and understanding the access and sustainment of the grassy ELM regime has been introduced. The exploration for type-II ELM regime in EAST has also been briefly introduced. In Sect. 3, recent advances in no-ELM H-mode regimes are presented, including an enhanced-recycling no-ELM regime, a non-inductive low-recycling no-ELM regime and a transient spontaneous no-ELM regime at relatively low pedestal collisionality ($\nu_e^* < 1$). In Sect. 4, small/no-ELM regimes achieved with impurity seeding are described. Section 5 gives summary and discussion.

2 Small ELM regime

The transient heat load caused by large-amplitude ELMs is a critical issue and thus should be well controlled for future fusion devices. The natural small ELM operation is one of the promising solutions. In the past decades, various small ELM regimes have been successfully developed in the worldwide (Viezzer 2018; Oyama et al. 2006; Stober et al. 2005; Maingi et al. 2011; Kamiya et al. 2007), including grassy (Kamada et al. 2000), type-II (Stober et al. 2001) and type-V ELMs (Maingi et al. 2005). The small grassy ELM regime has been developed since 2016 campaign in EAST (Xu et al. 2019; Yang et al. 2020), and the exploration for type-II ELM regime has also been conducted very recently under the lithium-coated wall.

This section will review the development of grassy ELM regime in EAST, and the exploration for type-II ELM operation will also be briefly introduced.

2.1 Typical small grassy ELMs in EAST

A typical EAST grassy ELM shot with an averaged ELM frequency $f_{\text{ELM}} \geq 2$ kHz is shown in Fig. 1. This shot is operated with plasma current $I_p = 400$ kA, magnetic field $B_t \sim 2.48$ T, poloidal beta $\beta_p \sim 1.8$, edge safety factor $q_{95} \sim 6.8$ and upper triangularity $\delta_u \sim 0.58$, under the upper signal null (USN) divertor configuration with an ITER-like upper tungsten divertor, in the unfavourable B_t , i.e. the ion ∇B drift away from the X-point. The total source heating power is ~ 9 MW, including 0.3 MW electron cyclotron resonance heating (ECRH), 0.6 MW lower hybrid current drive (LHCD) at 2.45 GHz, 1.7 MW LHCD at 4.6 GHz, 1.5 MW ion cyclotron resonance heating (ICRH), 4 MW co-current neutral beam injection (NBI) and 1.1 MW counter-current NBI. Good energy confinement has been obtained with $H_{98,y2} \sim 1.1$. The estimations from both peak heat fluxes onto the divertor target and edge extreme ultraviolet (XUV) radiations demonstrate that the ELM amplitude of grassy ELMs is only $\sim 10\%$ of that of type-I ELMs. In addition, the measurements of edge line-integrated density from POLarimeter-INTerferometer (POINT) diagnostic also indicate that the edge density reduction caused by grassy ELMs is usually less than the level of $\sim 0.3\%$, while for type-I ELMs it could be up to $> 5\%$.

It is necessary to assess whether the ELM amplitude of grassy ELMs is acceptable for future fusion devices or not. For ITER device, the ELM amplitude of

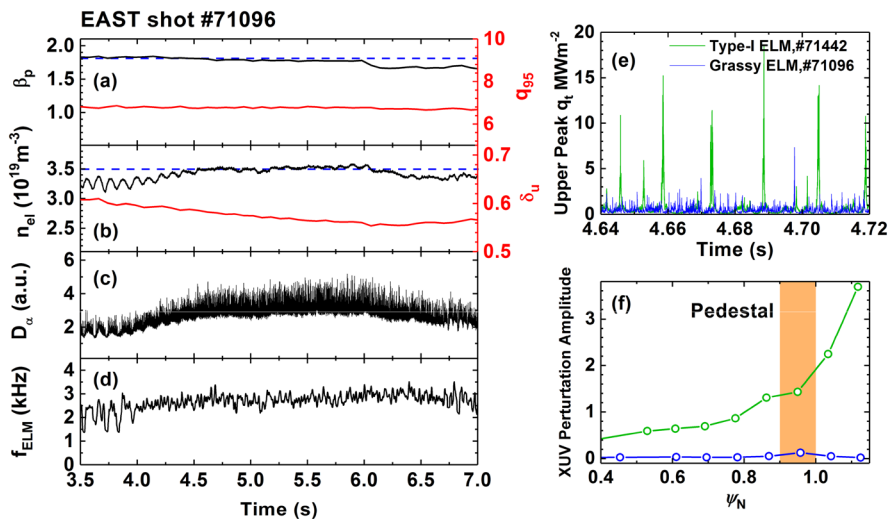
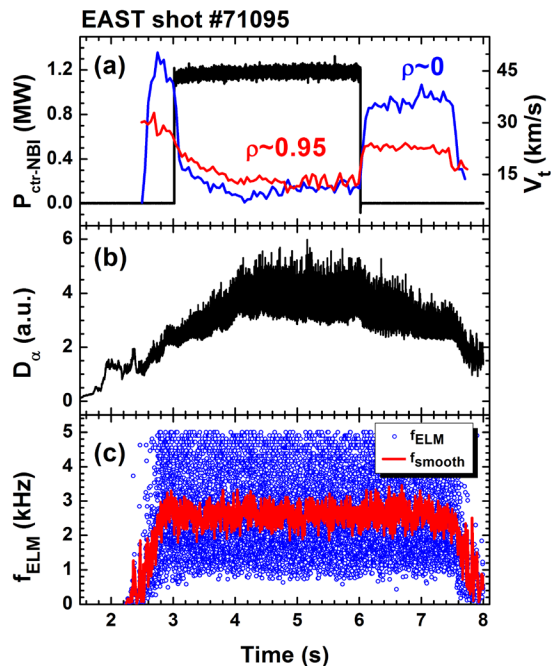


Fig. 1 A typical grassy ELM shot #71096 with $I_p = 400$ kA, $B_t \sim 2.48$ T and unfavourable B_t direction in EAST. Time histories of **a** poloidal beta β_p and edge safety factor q_{95} , **b** line-averaged density n_{el} and upper triangularity δ_u , **c** divertor D_α emission, and **d** ELM frequency f_{ELM} . **e** The peak heat fluxes on the divertor target plates and **f** edge XUV perturbation of grassy ELM in comparison to type-I ELM

type-I ELMs needs to be reduced to at least 1/20 for the protection of plasma facing material (Roth et al. 2009; Loarte et al. 2003b). Therefore, the ELM size of grassy ELMs is marginal. In order to further reduce the target energy fluence, the compatibility of the grassy ELM regime with highly radiative divertor needs to be performed, as suggested by Eich et al. (2017). For CFETR, the impact of the transient heat flux induced by grassy ELMs has also been studied, indicating that the energy fluence caused by a single grassy ELM pulse is below the tungsten melting limit, but tungsten erosion would exceed the material requirements (Li et al. 2021a). Therefore, external mitigation methods such as divertor detachment and advanced divertor geometry are suggested for the steady state operation of CFETR. The low rotation is expected in future reactor-size plasmas, and the compatibility of grassy ELM operation with the low plasma rotation has been demonstrated in EAST. As shown in Fig. 2, under the injection of counter-current NBI, both core ($\rho \sim 0$) and edge ($\rho \sim 0.95$) plasma toroidal rotations significantly decrease to a lower level of ~ 10 km/s. Meanwhile, the grassy ELM frequency and amplitude show no evident change, indicating that such small ELMs can be achieved under the condition of low plasma rotation. Higher β_p obtained by increasing either heating power or q_{95} is found to benefit a higher frequency of grassy ELM. Such high-frequency small ELM regime also exhibits a strong capability of tungsten impurity exhaust. In the accidental tungsten droplet events, the decay time of tungsten during grassy ELM shots is nearly 60% shorter than that in type-I ELM shots, suggesting much stronger tungsten impurity exhaust capability. The edge coherent mode (ECM) (Wang et al. 2014) and magnetic coherent mode (MCM) (Chen et al. 2018), which usually appear in the

Fig. 2 A demonstration of EAST grassy ELM operation compatible with low rotation. Time histories for EAST grassy ELM shot #70195 of **a** counter-current NBI power and toroidal rotations in the plasma core and edge regions, **b** divertor D_α emission and **c** f_{ELM} . This shot is operated with $I_p = 400$ kA, $B_t \sim 2.48$ T and unfavourable B_t direction



pedestal steep-gradient region in EAST, are dramatically weakened or even disappeared in grassy ELM discharges. Instead, a coherent mode with frequency ~ 20 kHz is sometimes observed near the pedestal top.

2.2 Operational window of grassy ELM regime in EAST

Grassy ELMs in EAST are highly reproducible in a wide range of operational parameters. Its operational space has been obtained by statistical analysis with a broad database covering almost all the grassy ELM shots in the 2016–2019 EAST campaign (Yang et al. 2020). q_{95} and β_p are found to be the two critical parameters for the access to grassy ELM regime in EAST. As illustrated in Fig. 3a, grassy ELMs with ELM frequency f_{ELM} larger than 500 Hz could be obtained when q_{95} and β_p are simultaneously high, i.e. $q_{95} \geq 5.3$ and $\beta_p \geq 1.2$. High q_{95} can dramatically reduce the risk of tokamak disruption (Garofalo et al. 2014) while high β_p facilitates the achievement of a high bootstrap current fraction. In addition, the high Shafranov shift at high β_p could also have a beneficial effect on the improvement of global energy confinement (Fukuyama et al. 1994). Good confinement with $H_{98,y2}$ up to 1.4 has been achieved with pure RF heating (LHCD+ECRH) in the grassy ELM discharges.

In EAST, grassy ELMs can be obtained under both favourable and unfavourable B_t configurations, and the access to the regime needs a relatively high heating power for a high β_p , but not rely on the heating methods like LHCD and NBI. Statistical analysis shows that different to the observations on JET (Saibene et al. 2005), the access to grassy ELMs is insensitive to high internal inductance l_i in EAST. The edge collisionality for the EAST grassy ELM regime is in the range $\nu_{e,\text{ped}}^* \sim 1\text{--}6$, and shows no evident difference with the collisionality space of large ELMs, i.e. $\nu_{e,\text{ped}}^* \sim 1\text{--}4$, here $\nu_{e,\text{ped}}^*$ is defined as (Sauter et al. 1999):

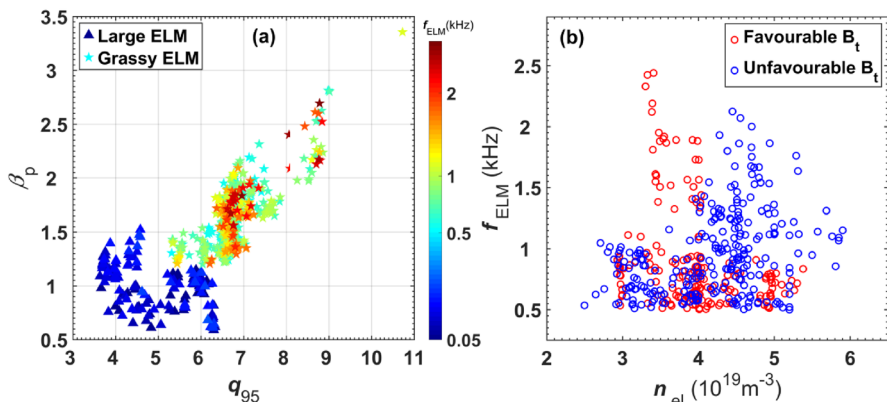


Fig. 3 **a** Parameter range of q_{95} and β_p for small grassy ELMs compared with large ELMs, **b** f_{ELM} as a function of plasma density in favourable and unfavourable B_t

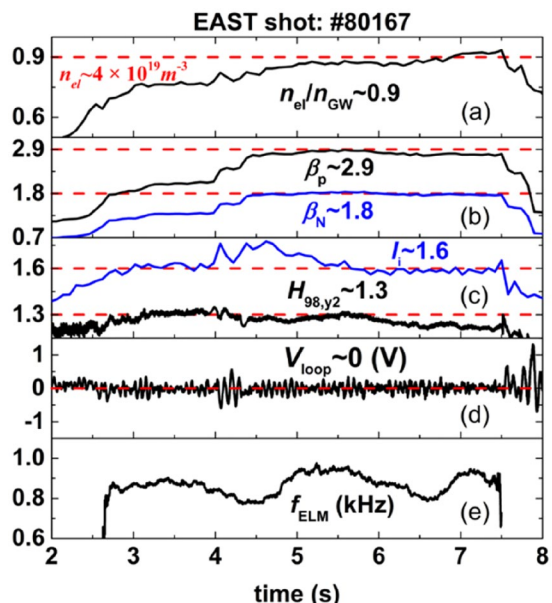
$v_{e,ped}^* = 6.921 \times 10^{-18} q_{95} R n_e Z_{eff} \ln \Lambda_e / (T_e^2 \epsilon^{3/2})$, where Z_{eff} , $\ln \Lambda_e$, ϵ are effective ion charge, Coulomb logarithm and inverse aspect ratio, respectively.

The grassy ELM regime shows good capacity of density control. The density range for EAST grassy ELM regime is fairly broad, i.e. $n_{el}/n_{GW} \gtrsim 0.45$. The lower density limit is only constrained by the NBI shine-through concern and tungsten guide limiters of RF antennas. No significant change in either the ELM behavior or energy confinement has been observed with a line-averaged density n_{el} up to $\sim 0.8 n_{GW}$. Higher β_p or triangularity are found to benefit the increase in grassy ELM frequency under unfavourable B_t configuration, while the grassy ELMs with high frequency ($f_{ELM} > 1$ kHz) are more dependent on the high plasma density in favourable B_t configuration as shown in Fig. 3b. Moreover, a phenomenon that the small grassy ELMs occur in clusters, named ‘clustered ELM’, appears to be more easily observed in favourable B_t configuration (Ding et al. 2021). Further investigations indicate that the occurrence of clustered ELM is closely related to the lower electron temperature ($T_{e,ped} = 200\text{--}400$ eV) compared to the non-clustered grassy ELMs in main plasma.

2.3 Compatibility of grassy ELMs with high bootstrap current fraction operation

The operational window of EAST grassy ELM regime has partly overlapped with the projected parameter range of the CFETR baseline scenario with 1 GW fusion power production (Yang et al. 2020). Actually, small grassy ELM scenario has been proposed as a promising ELM control solution for CFETR (Li et al. 2018; Zhuang et al. 2019). In addition to the aforementioned high density operation, high bootstrap current fraction operation is also needed to reduce the demands on external

Fig. 4 A typical EAST grassy-ELM, high- I_i , fully non-inductive shot #80167 with bootstrap current fraction $f_{BS} \sim 67\%$ at $q_{95} \sim 9$, $I_p = 300$ kA, $B_t \sim 2.48$ T, USN, unfavourable B_t . **a** Greenwald density fraction n_{el}/n_{GW} , **b** poloidal beta β_p , and normalized beta β_N , **c** internal inductance l_i and confinement enhancement factor $H_{98,y2}$, **d** loop voltage V_{loop} , and **e** ELM frequency f_{ELM}



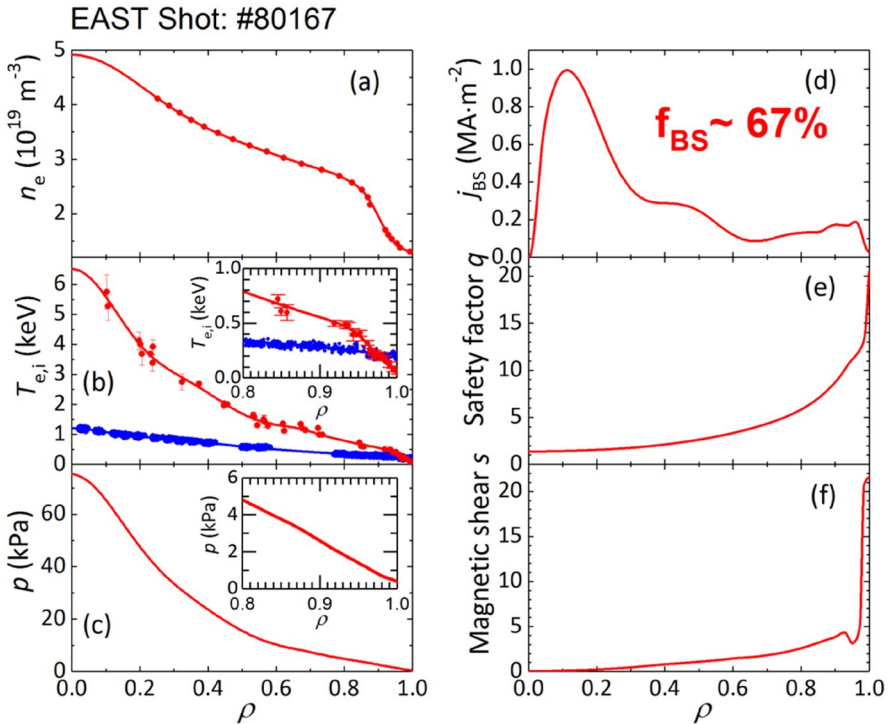


Fig. 5 Radial profiles at 5.7 s in a typical EAST grassy ELM, high I_p , fully non-inductive discharge #80167 with bootstrap current fraction $f_{BS} \sim 67\%$. **a** Electron density, **b** electron temperature (red) and ion temperature (blue), **c** total pressure, **d** bootstrap current density, **e** safety factor, and **f** magnetic shear

current drive for future fusion devices. Figure 4 shows a fully non-inductive discharge with high $q_{95} \sim 9$ and high $\beta_p \sim 2.9$, $I_p = 300$ kA, $B_t \sim 2.48$ T and unfavourable B_t direction. The total heating power includes 0.5 MW LHCD at 2.45 GHz, 1.9 MW LHCD at 4.6 GHz, 1 MW ECRH, 0.8 MW ICRH and 5 MW co-current NBI. The ELM frequency for the small grassy ELMs is 0.8–1 kHz. Figure 5 shows the typical radial profiles in this discharge. A larger density pedestal width than the T_e pedestal is observed at the edge, while the edge T_i is very flat without evident pedestal structure. In the plasma core the T_e is much higher than T_i as the electron-heating schemes LHCD and ECRH are the dominant heating powers. The kinetic EFIT equilibrium is reconstructed with bootstrap current given by the Sauter model (Sauter et al. 1999). Calculated with ONETWO code and confirmed by TRANSP code, high bootstrap current fraction of $f_{BS} \sim 67\%$ was obtained in this discharge with good energy confinement up to $H_{98,y2} \sim 1.3$ while $\sim 33\%$ of the plasma current was driven by the auxiliary heating systems. This discharge was obtained at quite high q_{95} , while $f_{BS} \sim 50\%$ can be achieved at CFETR relevant $q_{95} = 5.5\text{--}7$ in grassy regime (Zhuang et al. 2019). Accompanied with the upgrade of EAST heating system and relevant scenario development, the explorations for higher bootstrap current fraction will be conducted.

2.4 Compatibility of grassy ELMs with radiative divertor operation

Future tokamak reactors such as ITER and CFETR will be operated at metal wall, and thus the good control of stationary heat flux onto the divertor is also desirable in addition to the ELMs. Partial detachment operation with radiative divertor scenario has been considered as a primary solution for the control of divertor heat flux in ITER (Organization 2018). With the development of radiative divertor regime relevant techniques including the hardware and feedback control systems, the compatibility of grassy ELMs with radiative divertor operation has also been explored in EAST since the 2018 campaign (Li et al. 2020; Li et al. 2021b). Figure 6 shows a typical grassy ELM shot #87887 with stable partial detachment by using Ne impurity seeding while maintaining a good energy confinement. The electron temperature T_{et} near the upper outer strike point dramatically reduces with the seeding of gas mixture of 50% Ne and 50% D_2 from one single valve and is maintained $T_{et} = 5\text{--}8\text{ eV}$ by the feedback control scheme through pulse-width-modulated duty cycle of a piezo valve (Xu et al. 2020). Meanwhile, the divertor heat flux q_t decreases from ~ 1

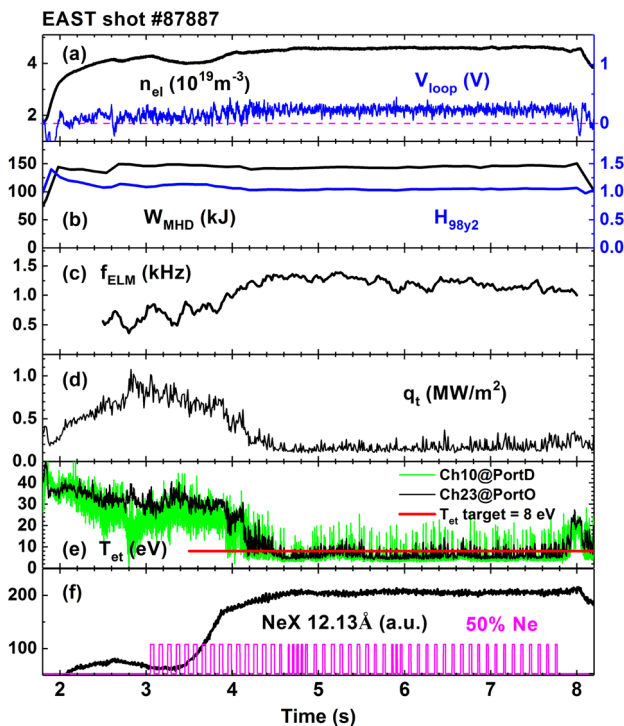


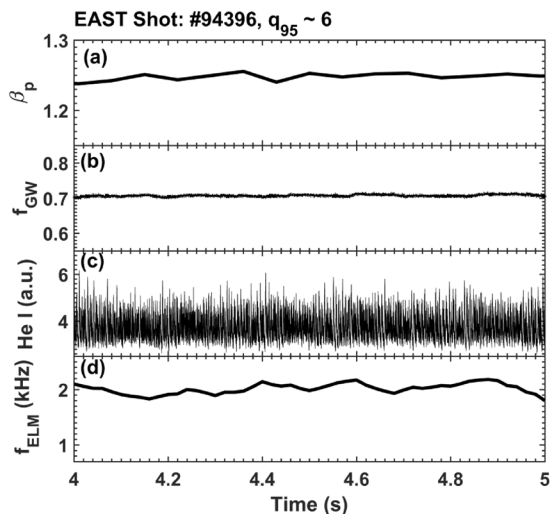
Fig. 6 The compatibility of grassy ELMs with the radiative divertor operation in EAST. Time histories for EAST shot #87887 of **a** plasma density and loop voltage, **b** stored energy and energy confinement factor $H_{98,y2}$, **c** ELM frequency, **d** divertor heat flux q_t , **e** electron temperature T_{et} in the vicinity of the upper outer strike point in the Port D and Port O, **f** Ne X emission and the voltage signal of piezo valve for Ne seeding. This shot is operated with $I_p = 400\text{ kA}$, $B_t \sim 2.42\text{ T}$, $q_{95} \sim 6.5$, favourable B_t

(MW/m²) to ~0.15 (MW/m²) with the divertor partial detachment. Note that, a good global energy confinement is well maintained with $H_{98,y2} > 1$ during the period of divertor detachment. Moreover, the ELM behavior becomes more grassy with ELM frequency increases from ~0.5 to > 1 kHz after Ne seeding. Such divertor detachment under grassy ELM H-mode plasma has also been obtained with the seeding of other impurity species, including Ar and CD₄ (Li et al. 2021b; Wu et al. 2021). These results demonstrate that the grassy ELM regime in combination with radiative divertor technique is a promising method for the simultaneous control of stationary and transient heat loads on future fusion device.

2.5 Grassy-like small ELMs in Helium plasma

Grassy-like small ELMs have also been observed in Helium (He) plasma in EAST. He plasma operation is expected to be conducted in ITER during the pre-fusion power operation phase (PFPO) and H-mode in the He plasma may be obtained in this period (Organization 2018). To support the ITER early pre-fusion power operation, He plasma experiments have been executed in 2018–2019 EAST campaign (Zhang et al. 2020). As shown in Fig. 7, the heating power in the He plasma discharge #94,396 includes 1 MW ECRH, 1.3 MW LHCD at 2.45 GHz, 2.6 MW LHCD at 4.6 GHz and 1.2 MW NBI. During the He plasma operation with He concentration ~70%, grassy-like high-frequency small ELMs can be observed from He I emissions at high $q_{95} \sim 6$, $\beta_p \sim 1.25$, $I_p = 450$ kA, $B_t \sim 2.4$ T, and favourable B_t with Greenwald density fraction of $f_{GW} \sim 0.7$. The ELM frequency is up to ~2 kHz. This result demonstrates that it is also promising to achieve grassy-like small ELMs in Helium plasma.

Fig. 7 Time histories for EAST grassy-like small ELM discharge #94396 during the He plasma operation with He concentration ~70% of **a** poloidal beta β_p , **b** Greenwald density fraction f_{GW} , **c** He I emission, **d** ELM frequency f_{ELM}



2.6 Underlying mechanism for small grassy ELMs

The physics mechanism for small grassy ELMs has been intensively investigated with the numerical simulations of ELITE and BOUT++ codes (Xu et al. 2019). Linear peeling–ballooning stability analysis indicates that the operational point of grassy ELMs is close to the peeling boundary, while the operational point of type-I ELM lies close to the corner. This is different from the grassy ELM regimes in JT-60U (Kamada et al. 2000), JET (Saibene et al. 2005) and AUG (Stober et al. 2005) or type-II ELMs (Stober et al. 2001), which were all concluded to be destabilized at the high- n ballooning stability boundary. Further nonlinear simulation has uncovered the physics mechanism of such small grassy ELMs. In the process of grassy ELM crash, both peeling and ballooning boundaries significantly expand and thus its operational point moves into the stable region after the initial pedestal collapse. The pedestal collapse stops and a small ELM is achieved. In contrast, the operational point in type-I ELM case is still located in the unstable region after the initial pedestal collapse. Pedestal continues collapsing and thus causes a large ELM eventually.

In comparison to type-I ELM regime, EAST grassy ELM regime has a wide pedestal, a flat density profile and a high ratio between the separatrix density and pedestal top density. The density ratio between the separatrix and pedestal top $n_{e,sep}/n_{e,ped}$ is high to $\sim 50\%$ for grassy ELM regime, whilst $n_{e,sep}/n_{e,ped}$ is $\sim 30\%$ for type-I ELM regime as shown in Fig. 8. There are several possible explanations for the formation of high separatrix n_e and moderate n_e gradient: (1) strong pedestal particle transport induced by the high-frequency grassy ELMs; (2) high neoclassical particle diffusion at high q_{95} ; (3) lithium wall coating reduces the recycling from the divertor and main chamber, thus reducing pedestal fueling. A significant increase of pedestal width, decrease of pedestal density gradient and suppression of ELMs have been observed in NSTX under the condition of lithium

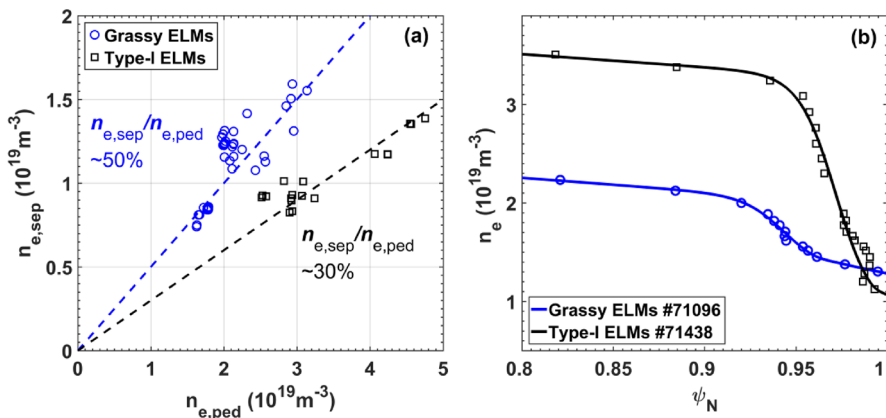


Fig. 8 **a** Separatrix density vs. pedestal top density and **b** typical pedestal density profiles for grassy ELMs and type-I ELMs in EAST

wall coating (Maingi et al. 2009). The high $n_{e,sep}$ and small density perturbations caused by grassy ELMs are essential for the metal wall environment, which facilitate impurity screening, divertor detachment with relatively low density at pedestal top and improve RF wave coupling.

2.7 Type-II ELMs in EAST

Another small ELM regime, i.e. type-II ELM, has also been observed in EAST recently. As shown in Fig. 9, the type-II ELM discharge #93820 was operated at relatively high Greenwald density fraction $f_{GW} \sim 0.65$, low $q_{95} \sim 4.5$, $\delta_u \sim 0.57$, $dR_{sep} \sim 3$ cm, $I_p = 450$ kA, $B_t \sim 1.75$ T in unfavourable B_t direction, USN divertor configuration. The heating power includes 0.5 MW LHCD at 2.45 GHz, 1.5 MW LHCD at 4.6 GHz, 3 MW co-current NBI and 1.4 MW counter-current NBI. The type-II ELM frequency is up to ~ 1 kHz. The characteristic broadband turbulence with frequency 10–30 kHz in the pedestal region could be clearly observed from the edge chord POINT measurements. Further EAST experiments indicate that higher plasma density facilitates the access to type-II ELMs, consistent with experimental observation on ASDEX-Upgrade (Stober et al. 2001). Although the number of type-II ELM discharges is very little in EAST, the typical experiments

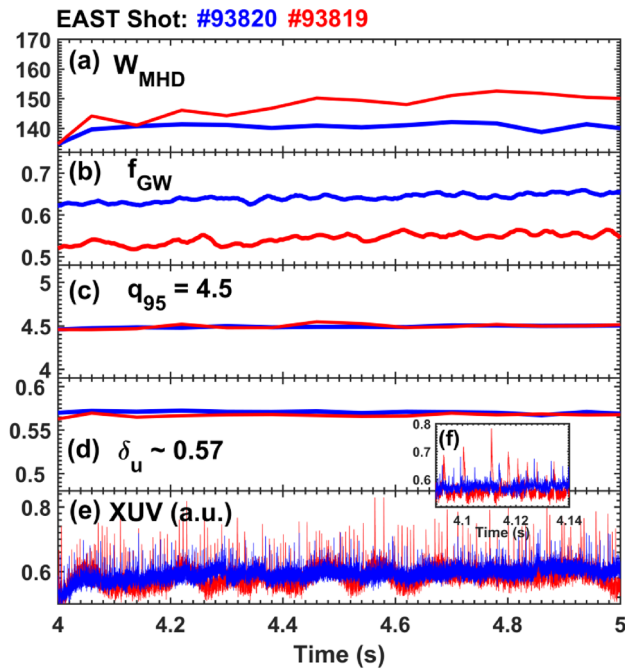


Fig. 9 Time traces for EAST type-II ELM discharge #93820 compared to #93819 of **a** stored energy, **b** Greenwald density fraction f_{GW} , **c** edge safety factor q_{95} , **d** upper triangularity δ_u , **e** edge XUV emission and **f** the zoom in on XUV emission

show that the ELM size of type-II ELM decreases with plasma density increasing, while the ELM size of grassy ELM regime increases with plasma density. More characteristics of EAST type-II ELM regime will be further explored in the future experimental campaign.

3 No-ELM regime

In this section, the characteristics and physical mechanisms of three spontaneous no-ELM H-mode regimes frequently observed in EAST will be introduced.

(1) The first one is an enhanced-recycling H-mode regime, which appears at relatively high pedestal collisionality ($\nu_e^* > 1$) under the conditions of RF-dominated heating and lithium wall coating. This regime has an enhanced divertor D_α emission and a high- n (toroidal mode number $n = 17\text{--}20$) electrostatic Edge Coherent Mode (ECM) driving significant pedestal particle and heat transport (Wang et al. 2014; Ye et al. 2017). This regime is quite similar to the enhanced D_α H-mode (EDA) observed in Alcator C-Mod (Greenwald et al. 1999) and the high recycling steady H-mode (HRS) in JFT-2 M (Kamiya et al. 2004). This regime was firstly achieved in 2012, and then successfully demonstrated its compatibility with the fully non-inductive long-pulse (> 15 s, 10–20 times longer than the current diffusion time) operation in the 2014 EAST experimental campaign (Ye et al. 2017). The good energy confinement performance ($H_{98,y2} \sim 1.2$), good impurity control, and relatively high Greenwald density fraction ($\langle n_e \rangle / n_{GW} \sim 0.5$) were achieved simultaneously in the long-pulse demonstration experiments (Ye et al. 2017). The increase of the pedestal width, local flattening of the density profile near the separatrix and shift of the peak gradient region radially inward result in the expansion of the ballooning instability boundary and thus improved pedestal height and energy confinement performance. The combined effect of density pump-out induced by ECM and edge plasma ergodization induced by LHW is thought to be the cause of these profile changes (Liang et al. 2013).

Statistical research shows that the stationary no-ELM H-mode plasma has been obtained mostly with 4.6 GHz LHW heating or counter-current NBI plus ECRH, in suitable configuration (elongation $\kappa = 1.55\text{--}1.63$ and outer gap = 3.5–5.5 cm). With additional power from co-current NBI, ICRF or 2.45 GHz LHW, or even a slightly increase in plasma elongation or outer gap from the compatible window, ELMs appear, but they are mostly small ELMs (Ye et al. 2017). In addition, researches of the ECM, which plays a key role in this regime, have been carefully carried out in EAST in recent years. ECM is an electrostatic instability, with a rather weak magnetic component, $\delta B \sim 0.2G$ ($\delta B/B_p \sim 1 \times 10^{-4}$), as measured by small magnetic coils mounted on the reciprocating probe and moved radially to be located transiently (several tens of ms) slightly outside the separatrix (~ 5 mm), where ECM can be touched (Wang et al. 2014). ECM is observed to be located in the steep-gradient pedestal region, which propagates in the electron diamagnetic drift direction in the laboratory frame, and exhibits ballooning-like structure. GYRO, BOUT++ and GTC simulations consistently suggested that the ECM may have the same nature of the dissipative trapped electron mode (DTEM) (Wang et al. 2014; Xia et al. 2017;

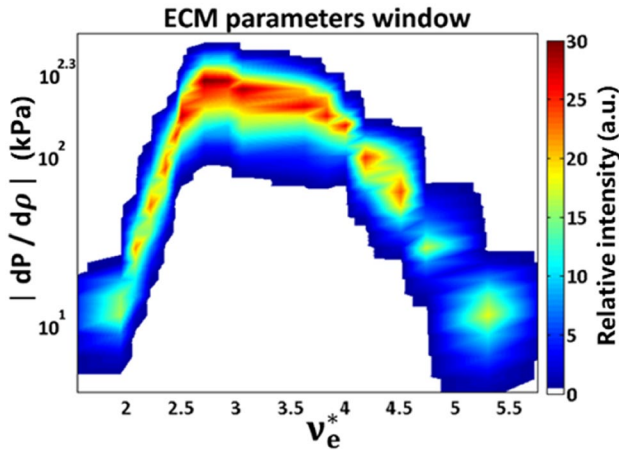


Fig. 10 ECM parameter space in EAST obtained from 28 individual shots, the abscissa is pedestal collisionality, the ordinate is the pressure gradient, and the color contour levels represent the relative intensity of the ECM. Reprinted from Ye et al. (2017). Copyright 2017 IOP

Zhao et al. 2017). As demonstrated by statistical analysis, the ECM is strongly correlated with the pedestal collisionality and the pressure gradient, with the suitable operating space of the collisionality ranges from 2.5 to 5 and the pressure gradient ranges from 100 to 200 kPa ($dP/d\rho$, where ρ is the square root of the normalized poloidal magnetic flux), as shown in Fig. 10 below, consistent with the simulations.

(2) The second one is a non-inductive low-recycling H-mode regime, which is achieved under the conditions of RF-dominated heating (mainly LHCD) and extensive lithium wall coating (30 g for each time, usually twice the amount than the normal case) or during real-time lithium powder/granules injection at relatively low heating power (Ye et al. 2019). The salient feature of this no-ELM regime is that the edge D_α emission intensity, the separatrix electron density, divertor recycled neutral particles and the pedestal fueling are significantly reduced after the L–H transition, the amplitude of the ELMs continues to decrease until they disappear completely. Unlike the high-recycling no-ELM regime with strong ECM as mentioned above, this regime has no clear correlation with the pedestal fluctuations. Another difference is that this regime is more likely to be obtained at relatively low electron density and the density threshold varies with magnetic field, coating thickness and plasma current (Ye et al. 2019).

ELITE and NIMROD simulations show that different from the lithium-conditioned no-ELM regime in NSTX which is caused by the density profile modification (Maingi et al. 2009) or the increased effective charge number Z_{eff} (Debabrata et al. 2017), the enhanced ion diamagnetic stabilization of intermediate- n and high- n PBMs with decreasing separatrix density is the key to enter this regime in EAST. This no-ELM regime can transfer into a stationary low-heating power small-ELMs regime with the divertor peak heat flux lower than 4 MW/m^2 (average heat flux lower than 1.5 MW/m^2) by increasing the density at pedestal foot through high frequency ($\sim 1 \text{ kHz}$) and short-pulse ($\sim 1 \text{ ms}$ with velocity $\sim 1 \text{ km/s}$) supersonic

molecular beam injection (SMBI). The small ELMs, which seems to be not grassy ELMs, greatly facilitate impurity control and nearly fully non-inductive operation (loop voltage < 0.1 V), which is critical for achieving long-pulse H-mode operations. The record 101 s H-mode plasma was obtained in this small ELM regime with real-time lithium powder injection (several milligrams used in this discharge and Z_{eff} around 3) in the 2017 EAST experimental campaign, as shown in Fig. 11 below (Wan et al. 2019; Gong et al. 2019).

(3) The third one is a transient spontaneous no-ELM regime obtained at high heating power (source power ~ 7 MW including co-current NBI and LHW) and low pedestal collisionality ($\nu_e^* < 1$), with a stronger and more coherent low- n (mostly $n=1$) Magnetic Coherent Mode (MCM) but without ECM (Zhang et al. 2019), as shown in Fig. 12. The MCM is characterized by strong magnetic fluctuations as measured by high frequency Mirnov coils mounted on the wall and very weak density fluctuations. MCM is one of the most common pedestal fluctuating modes in EAST. Its parameter space covers broad ranges, in particular, the different heating schemes (LHCD alone, NBI only (co-current NBI, counter-current NBI or mixed NBI) or with additional heating power from ECRH and ICRF), different wall materials (full C in 2010, C divertor plus Mo first wall in 2012 and C lower divertor plus W upper divertor plus Mo first wall since 2014) and different wall conditioning (lithium or silicon coating), but not in very low- T_e or highly collisionality pedestal which is typical in type-III ELMy H-mode phase. Dedicated experiments have been conducted in recent years in EAST to study the physical mechanism behind MCM. Density ramping up experiments exhibit a good linear scaling of the MCM frequency with the local toroidal Alfvén Eigenmode (TAE) frequency, suggesting the MCM may have the same nature of TAE modes. The MCM frequency was also observed to decrease during plasma current (I_p) ramping down, i.e., edge safety

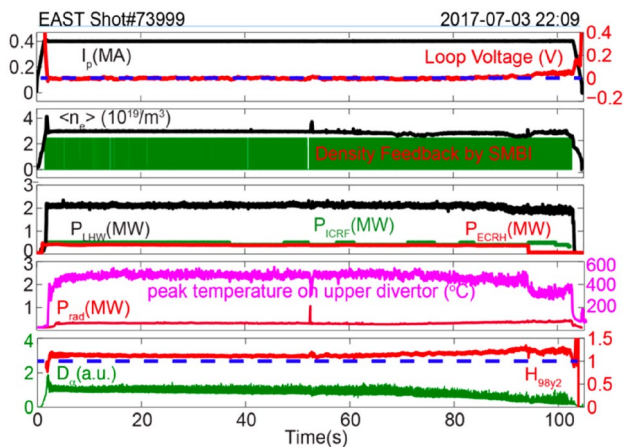


Fig. 11 The record 101 s long-pulse H-mode in EAST. From top to bottom are plasma current, loop voltage, line-averaged electron density, auxiliary heating power of ECRH, ICRF and LHW, divertor temperature, radiation power, energy confinement factor $H_{98,y2}$ and D_α emission intensity. This shot is achieved at $I_p = 400$ kA, $B_t \sim 2.5$ T, and unfavourable B_t . Reprinted from Ref. (Wan et al. 2019). Copyright 2019 IOP

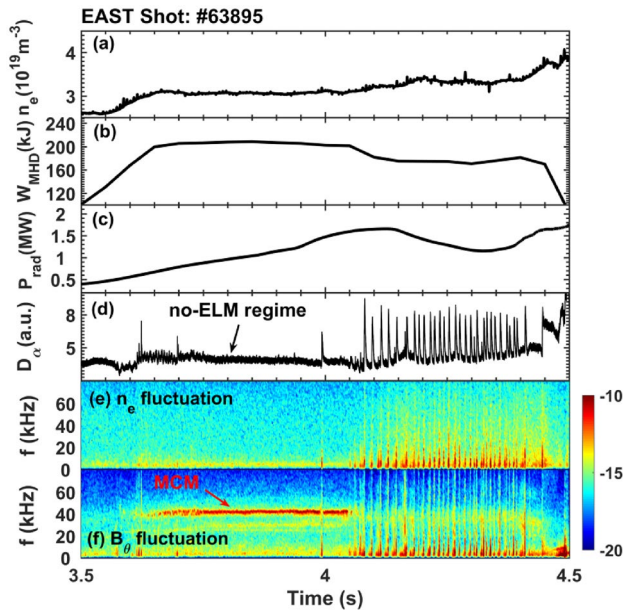


Fig. 12 Time traces of **a** plasma density, **b** stored energy, **c** radiated power in the main plasma, **d** D_{α} emission, **e** pedestal density fluctuation and **f** magnetic fluctuation showing MCM for the shot #63895 of transient spontaneous no-ELM regime on EAST

factor q_{95} ramping up. This phenomenon can be explained by a continuous radially inward shift of TAE gap up the pedestal density gradient (Chen et al. 2018; Xu 2017).

However, MCM cannot drive effective pedestal transport due to its weak electrostatic fluctuating and very small poloidal wavenumber. The impurity exhaust capability, especially the high- Z impurities, is insufficient in this no-ELM regime, which makes it unable to maintain a long-pulse operation.

4 Impact of impurity injection on small/no-ELM regimes

The radiative divertor scenario with impurity seeding has been demonstrated to be an effective method to reduce the stationary power load on divertor targets that is planned to be applied in ITER (ITER Organization 2018; Doyle et al. 2007). It has been recognized that radiative divertor regime can not only control the stationary particle and heat fluxes but also have a significant impact on the ELM behavior. The radiative divertor experiments on JET with the carbon wall (Beurskens et al. 2008), JT-60U (Asakura et al. 2009) and DIII-D (Wang et al. 2017) have shown that a transition from type-I to type-III ELMs would occur with excessive impurity being injected. By using nitrogen seeding, the mitigation of type-I ELMs has been observed in the ASDEX-Upgrade tokamak (Schneider et al. 2014). More excitingly, JET tokamak with ITER-like wall has recently demonstrated a small ELM regime

with high confinement at low q_{95} and low pedestal collisionality through three methods, and one of these methods is operation with low gas fueling, pellet injection and a small amount of Ne injection (Garcia et al. 2022). In addition, the HL-2A experiments with Ne injection demonstrated that the change of ELM behaviour is very sensitive to the impurity ratio of the injected mixture gas (Zhong et al. 2019). Overall speaking, impurity injection can strongly affect the ELM behaviour which attracts extensive attention.

In the past few years, radiative divertor technique was developed for the active control of divertor heat load in EAST under the H-mode background plasmas with various ELM types, and different changes of ELM behavior with impurity injection have been observed in the experimental series (Xu et al. 2020; Li et al. 2021b; Lin et al. 2022; Ye et al. 2021). In this section, the impurity-injected experiments with the phenomena of ELM transition from type-III to large ELMs, ELM transition from mixed to grassy ELMs, and ELM suppression are briefly described.

4.1 Different ELM responses to impurity injection

An anomalous phenomenon of ELM behavior changing from type-III to low-frequency large ELMs induced by Ne injection was obtained in the H-mode plasma at

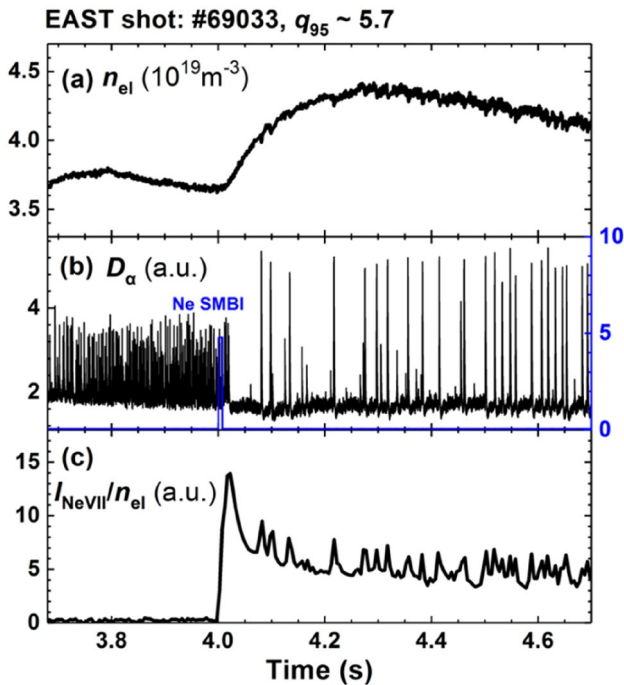


Fig. 13 EAST experiment with ELM behavior changing from type-III ELM to large ELM induced by Ne injection. Time traces of **a** plasma density, **b** divertor D_α emission and monitor of the Ne impurity pulse, and **c** intensity of Ne VII emission in the bulk plasma for shot #69033

marginal q_{95} space during the development of radiative divertor regime in EAST (Lin et al. 2022). As shown in Fig. 13, the background plasma of shot #69033 is the H-mode with type-III ELMs, operated at $I_p=500$ kA, $B_t\sim 2.5$ T, low $\beta_p\sim 0.9$ and $q_{95}\sim 5.7$, unfavourable B_t in USN configuration. Note that, the q_{95} in the shot is in the marginal q_{95} space (i.e. $q_{95}\sim 5.2\text{--}6.4$) in which both large ELM and small ELM could be observed (Yang et al. 2020). With the injection of a short pure Ne gas pulse by SMBI, unexpectedly, the type-III ELMs with $f_{\text{ELM}}\sim 500$ Hz disappear completely, and the ELM behavior changes to the large ELMs with lower $f_{\text{ELM}}\sim 55$ Hz. In the pedestal region, the density gradient increases dramatically while the pedestal electron temperature decreases from 490 to 420 eV, consequently, the pedestal collisionality $\nu_{e,\text{ped}}^*$ increases from 1.9 to 3, the pressure gradient increases modestly and edge bootstrap current shows little change. Further analyses in experiments and simulations indicate that, the dramatic increase in pedestal density gradient could play the dominant role in the observed ELM behavior change in this case. These results may facilitate a deeper understanding of the role of edge density gradient on the peeling–ballooning instabilities and the ELM activity.

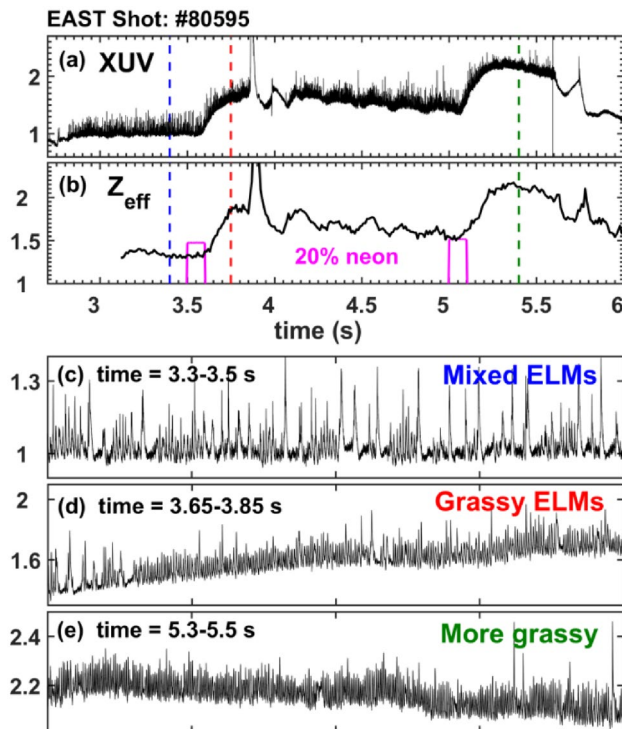


Fig. 14 EAST experiment with ELM behavior changing from mixed ELMs to high-frequency grassy ELMs induced by Ne seeding. Time traces for shot #80595 of **a** edge XUV radiation, **b** effective charge number Z_{eff} and the monitor of the impurity pulse. The zoom in on XUV radiation in the periods of **c** 3.3–3.5 s, **d** 3.65–3.85 s, **e** 5.3–5.5 s

Different to the aforementioned ELM response to impurity injection, the ELM behavior changing from mixed small and large ELMs to pure grassy ELMs has also been observed by using Ne seeding during the expansion of operational parameter space of grassy ELM regime towards lower q_{95} in EAST (Li et al. 2020). As shown in Fig. 14, the shot #80595 is operated with $I_p=450$ kA, $B_t\sim 2.25$ T, relatively high $\beta_p\sim 1.5$ and $q_{95}\sim 5.7$, unfavourable B_t , in the USN configuration. The operational parameter q_{95} is also in the marginal q_{95} space of large and small ELMs, hence the mixed ELMs with averaged frequency $f_{ELM}\sim 500$ Hz have been observed before Ne seeding. With the mixture impurity seeding of 20% Ne and 80% D₂, the ELM behavior becomes grassy ELMs and the ELM frequency increases to $f_{ELM}\sim 1.2$ kHz simultaneously. Moreover, the ELM behavior becomes even more grassy with higher frequency of $f_{ELM}\sim 1.6$ kHz after the injection of second Ne pulse. Note that similar ELM mitigation with the transition from large ELMs to high-frequency grassy ELMs induced by impurity seeding was also achieved at the marginal q_{95} space during the He plasma operation. These results provide a new approach to the small ELM regime exploration towards ITER-relevant low q_{95} ($q_{95}\sim 3$) in EAST.

4.2 No-ELM regime induced by impurity injection

In 2019, a highly reproducible no-ELM H-mode regime under the condition of radiative divertor has been observed through deuterated methane (CD₄) injection in EAST (Xu 2020). Figure 15 shows typical discharge information of ELM suppression and partial detachment (inner target) achieved with CD₄ seeding in EAST. It can be seen that, the ELM suppression occurs (Fig. 15b) when the carbon 6+ line emission intensity I_{C6+} (Fig. 15a) exceeds a certain threshold level. The energy confinement factor $H_{98,y2}$ is reduced by 10% and the plasma stored energy W_{MHD} is nearly maintained (Fig. 15c). A low n ($n=1$) mode as well as its harmonics in the H-mode plasmas is excited after CD₄ injection from the upper outer divertor near the striking point with sufficiently high impurity concentration (Fig. 15f), initiating from the oscillation of a radiation belt in the high-field-side SOL region near the X-point. Unlike the edge harmonic oscillation (EHO) in the quiescent H-mode (QH-mode), the $n=1$ mode is strongly related to the impurity concentration near X-point and electron temperature near divertor target plate surface. This mode is also located near X-point and difficult to penetrate into the pedestal top region. Note that it's difficult in EAST to measure the impurity concentration. We use the line emission intensity of C⁶⁺ to reflect the relative C impurity concentration in the CD₄ injection experiments. The impurity concentration for exciting the $n=1$ mode is similar to that for divertor detachment. ELM suppression has been robustly achieved accompanied by this mode in a wide q_{95} window from 4.5 to 6.5 ($B_t=2.25, 2.47$ T in favourable or unfavourable direction and $I_p=400\text{--}600$ kA) and a wide heating power range with source power from 3 up to 9 MW. In the typical discharge with CD₄ seeding, it appears that the $T_{e,ped}$ decreases and v_e^* increases. Divertor partial detachment has also been achieved along with ELM suppression with significant reduction in ion saturation current at the inner divertor target plate and target electron temperature $T_{et} < 10$ eV (Fig. 15d). In addition, active feedback control of either

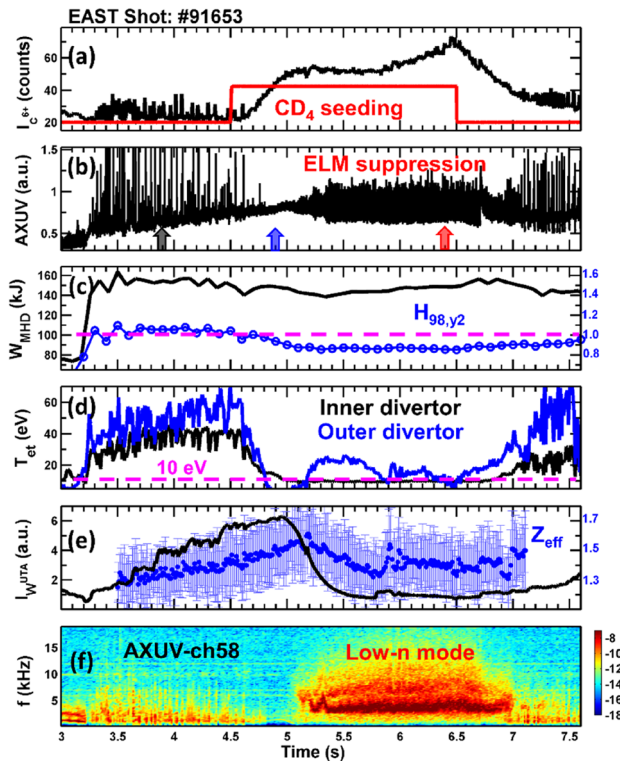


Fig. 15 Typical discharge information of ELM suppression and partial detachment (inner target) achieved with CD_4 seeding in EAST, including **a** carbon 6+ line emission intensity (black) and CD_4 gas valve voltage (red), **b** AXUV (ch58, near the upper X-point area) signal, **c** plasma stored energy W_{MHD} and energy confinement factor $H_{98,y2}$, **d** target electron temperature near the inner (black) and outer (blue) strike point measured by divertor Langmuir probes, **e** core tungsten W27+ to W45+ line emission intensity measured by an EUV system and the effective charge number Z_{eff} measured by a VB system and **f** power spectra measured by AXUV (ch58). Reprinted from Ref. (Ye et al. 2021). Copyright 2021 IOP

divertor radiation or T_{et} with CD_4 injection has been achieved, for the first time, in this regime (Xu 2020; Ye et al. 2021). This $n=1$ mode exhibits strong particle transport and high- Z impurity exhaust capability (Fig. 15e), contributing to the long-pulse sustainment of this no-ELM state.

In addition, this $n=1$ mode is independent on the specific impurity species, which can also be observed with helium, lithium, boron, neon or argon injection, in a sufficiently high impurity concentration but with different excitation difficulty in EAST (Xu 2020; Sun et al. 2021). The nature of this $n=1$ mode is still unclear and attention has been paid to two hypotheses, (1) the first one is that the mode is driven by the coupling of the impurity radiative condensation instability and drift waves (Xu et al. 2020), and (2) the second one is that the mode is a type of geodesic acoustic mode driven by density perturbation at the X-point area (Diallo 2020).

5 Summary and discussion

One challenge in steady-state and high-performance operation in future tokamak fusion reactors is to develop H-mode operational regimes that mitigate or eliminate the large-amplitude ELMs to decrease the transient heat flux on the divertor and first wall. The small/no-ELM regimes, characterized by sufficiently small transient heat flux and sufficient ELM impurity exhaust, have been considered as a viable solution to this challenge. A great deal of effort has been directed to the development of small/no-ELM regimes in EAST and significant progress in extending and understanding the access and sustainment of the small/no-ELM regimes has been obtained. This paper reviews the recent advances in developing natural and impurity-induced small/no-ELM H-mode regimes in EAST. A brief summary of these regimes is given in Table 1.

Highly reproducible stationary grassy ELM regime with good energy confinement and excellent tungsten impurity exhaust capability has been obtained in EAST with water-cooled metal wall, compatible with low rotation, high normalized density, high bootstrap current fraction, radiative divertor and fully non-inductive operations. These conditions would be also required for future fusion reactor-level plasmas. Grassy-like small-ELM H-mode regime has been achieved in He plasma experiments, which will be conducted during the pre-fusion power operation phase in ITER. The grassy ELM regime is thought to be a potential operational regime for future tokamak fusion reactors. The high-frequency small-amplitude grassy ELMs could drive strong cross-field particle transport, which facilitates the achievement of a high $n_{e,sep}/n_{e,top}$ and a high SOL density. The high SOL density would help to screen the edge impurities in the grassy ELM regime. With the aid of the strong particle exhaust and high-Z impurity control due to the grassy-ELM-driven filamentary transport, the grassy ELM regime becomes especially suitable for steady-state operation with radiative divertor and metal first wall. The wide pedestal at high β_p and low rotation is expected in future fusion reactor-level plasmas, which leads to low pedestal bootstrap current density and thus more stable kink/peeling modes in the pedestal region. Nonlinear simulations of the grassy ELM burst event have found that the peeling–ballooning instability boundary would expand after an initial localized crash in the pedestal region, which helps to improve pedestal stability against PBMs and avoid large-amplitude ELM bursts (Xu et al. 2019). These new findings will greatly enhance the confidence to apply this regime as a baseline scenario to CFETR and other steady-state tokamak fusion reactors. However, compared with the operation region of the steady-state scenario of CFETR with 1 GW fusion power production (Zhuang et al. 2019), the operation region of pedestal collisionality in the grassy ELM regime in EAST is relatively high, i.e. $\nu_e^* \sim 1-6$. This is mainly limited by the heating power available in EAST. To further develop the predictive capability towards future fusion reactors, it's necessary for us to extend the grassy ELM regime in EAST to lower pedestal collisionality region in future work. In addition, the small ELM regime, i.e. type-II ELM regime, has also been observed in EAST, along with a characteristic broadband turbulence with frequency of 10–30 kHz in the pedestal

Table 1 A brief summary of small/no-ELM H-mode regimes in EAST

Devices		EAST							CFETR (Zhuang et al. 2019)
Regimes	Grassy ELM regime	Type-II ELM regime	Enhanced-recycling no-ELM H-mode regime	Low recycling no-ELM H-mode regime	Transient spontaneous no-ELM regime	Impurity-induced no-ELM regime	I GW steady-state operation		
Operation region	v_e^* q_{95} β_p κ δ f_{GW}	~ 2 ~ 4.5 ~ 1.1 ~ 1.7 ~ 0.43 ~ 0.65	$\sim 2.5-4$ $5.5-6.5$ $1.1-1.4$ $1.55-1.65$ -0.45 -0.5	> 1 $5.5-6.5$ $0.7-1.2$ $1.58-1.64$ $0.36-0.42$ $0.35-0.5$	$-0.8-1$ -5.4 -1.3 -1.6 -0.45 -0.45	≥ 1 $\sim 4.6-6.5$ $-0.9-1.7$ ~ 1.6 -0.4 $0.3-0.9$	≥ 1 $\sim 4.6-6.5$ $-0.9-1.7$ ~ 1.6 -0.4 $0.3-0.9$	~ 0.15 5.54 2.1 2.0 0.42 0.57	
Pedestal/edge fluctuations	A coherent mode with ~ 20 kHz can be observed near pedestal top sometimes	Broadband turbulence	ECM dominated	No clear correlation with pedestal fluctuations	MCM	$n = 1$ mode with its harmonics			
Access requirement	High q_{95} , high β_p and a wide pedestal with low density gradient	High plasma density	High recycling, RF-dominated heating and lithium wall coating	RF-dominated heating, strong lithium coating or lithium powder/granules injection	High heating power and low v_e^*	Sufficiently high impurity concentration near X-point			

Table 1 (continued)

Devices		EAST				CFETR (Zhuang et al. 2019)
Regimes	Grassy ELM regime	Type-II ELM regime	Enhanced-recycling no-ELM H-mode regime	Low recycling no-ELM H-mode regime	Transient spontaneous no-ELM regime	Impurity-induced no-ELM regime
Advantages	Compatible with good energy confinement, steady-state operation, low rotation, high density, high bootstrap current fraction and radiative divertor; Strong capability in the exhaust of high-Z impurities	Compatible with high density	Compatible with good energy confinement, steady-state operation, high density; Good capability in impurity control	Compatible with good energy confinement, long-pulse operation	Compatible with relatively low v_e^*	Compatible with radiative divertor and long-pulse operation; Achieved with a variety of impurity species
Key concerns	Needs to be extended to lower v_e^*	No systematic research in EAST	Not compatible with low v_e^*	Not compatible with high density	Unable to maintain a long-pulse operation	Needs to be extended to lower v_e^*

region. More characteristics of EAST type-II ELM regime will be further explored in the future experimental campaign.

Three spontaneous high confinement no-ELM regimes frequently observed in EAST have been introduced, including an enhanced-recycling H-mode regime observed at relatively high pedestal collisionality ($\nu_e^* > 1$) with lithium wall coating and RF-dominated heating, a non-inductive low-recycling H-mode regime observed under the conditions of extensive lithium wall coating and RF-dominated heating (mainly LHCD) or during real-time lithium powder/granules injection at relatively low heating power, and a transient spontaneous no-ELM regime obtained at high heating power (source power ~ 7 MW) and relatively low pedestal collisionality ($\nu_e^* < 1$). It has been found that the enhanced-recycling no-ELM H-mode regime is strongly correlated with the high- n ECM driving significant particle and heat transport, which is an electrostatic instability and thought to have the same nature of the DTEM. The ECM in the pedestal region helps the local flattening of the separatrix density gradient, shift of the peak gradient region radially inward and increase of the pedestal width and thus the expansion of the ballooning stability, which leads to enhanced pedestal height and global energy confinement. However, due to the strong dependency of ECM on relatively high pedestal collisionality, i.e. $\nu_e^* \sim 2.5\text{--}4$, this regime seems to be not suitable for future fusion reactors with lower pedestal collisionality. The non-inductive low-recycling no-ELM H-mode regime doesn't show clear correlation with the pedestal fluctuation. The decrease in separatrix density and thus enhanced ion diamagnetic stabilization have been suggested to be the key in access to this regime. This regime is more likely to be obtained at relatively low electron density and thus might be difficult to be compatible with high plasma density in future fusion reactors. The transient spontaneous no-ELM H-mode regime is correlated with low- n MCM instead of ECM, which shows very weak density fluctuation and particle exhaust capability, especially the high- Z impurities, and appears to be not conducive to the sustainment of this regime. This no-ELM regime appears not to be applicable for the long-pulse operation in future reactors.

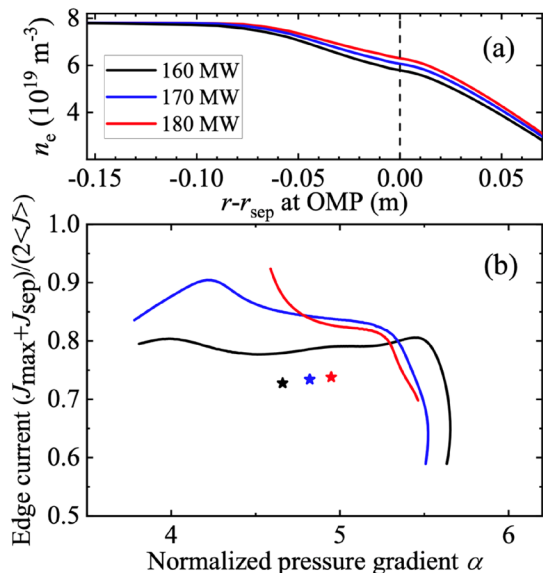
In addition, small/no-ELM regimes with impurity injection in EAST have been achieved and shown to be compatible with radiative divertor. The ELM behavior changing from mixed small and large ELMs to pure grassy ELMs has been observed with Ne seeding. While an anomalous transition from type-III to low-frequency large-amplitude ELMs induced by Ne injection has also been observed in the radiative divertor experiments in EAST. The no-ELM regime with CD_4 injection has been achieved robustly in the presence of an $n=1$ mode in the high-field-side region near the X-point, which exhibits strong particle transport and high- Z impurity exhaust capability and facilitates the sustainment of the long-pulse no-ELM state. However, the pedestal collisionality in this regime is relatively high, i.e. $\nu_e^*/1$, and it's also necessary to extend this regime to lower pedestal collisionality in our future work.

The compatibility with divertor detachment operation is a key issue for the application of the small/no ELM regimes on future fusion reactors. In the past few years, a series of radiative divertor experiments have been performed in EAST, and partial detachment operation has been achieved in the grassy ELM regime. The full detachment with particle and heat fluxes on the whole divertor well controlled has not

been obtained in EAST by now, as it is easy for confinement degradation and even disruption when extending the partial detachment to full detachment only by using impurity seeding. In the future work, we would combine the density ramping up and impurity seeding to explore full detachment under the small grassy ELM regime, as well as other small/no-ELM regimes.

In summary, the prospects of the small/no-ELM H-mode regimes are very promising and significant progress in extending and understanding the access and sustainment of these regimes has been made recently in EAST. Although the different small/no-ELM H-mode regimes reviewed in this paper all have different characteristics, they all exhibit characteristic pedestal or edge fluctuations. There seems to be an underlying mechanism behind these small/no-ELM H-mode regimes, which could help drive pedestal transport and thus change pedestal structure, making the PBMs more stable and as a result, no type-I ELMs occur. Besides, the pedestals characterized by wide density pedestal and low density gradient in these regimes help to stabilize PBMs. The density pedestal gradient in future fusion reactor-level plasmas could be even lower. There are two main factors leading to flat density profile in the pedestal: low particle source and strong particle exhaust in the pedestal, which both exist in future reactor-level grassy-ELM plasmas. The plasma density and temperature near the separatrix are expected to be very high in future reactor-level plasmas and the recycling neutrals would be ionized mostly in the SOL and divertor region, so the penetration into the pedestal is almost negligible (Romanelli et al. 2015). Hence, low particle source in the pedestal is very likely achievable with deep fueling using the high-field-side high-speed injection of large-size pellets (Vincenzi et al. 2015). With the aid of pedestal particle exhaust driven by edge localized instabilities, a flat density pedestal profile with high SOL density is expected as well as a relatively

Fig. 16 **a** Electron density n_e profiles obtained at different input powers P_{input} imposed with the SOLPS code and **b** corresponding pedestal stability diagram are shown. r_{sep} is the minor radius of the separatrix. The dashed line represents the separatrix. Reprinted from Wang et al. (2021). Copyright 2021 IOP



low peak bootstrap current density since the density gradient is the main contribution to the bootstrap current density (Sauter et al. 1999). As shown in Fig. 16, SOLPS simulation indicates that the separatrix density would increase with the heating power in CFETR. ELM instability analysis by ELITE code suggests that the ballooning instability boundary narrows and the operational point moves closer to the ballooning boundary with flatter density profile, which is thought to facilitate the achievement of small ELM regime (Wang et al. 2021). These new findings will greatly enhance the confidence to apply the small/no H-mode regimes to future steady-state tokamak fusion reactors.

However, a full understanding of what sets the density pedestal structure is still not available. Inward particle pinch could also play a role in determining the density pedestal structure in future high opacity plasmas (Mordijck 2020). In addition, a detailed physics understanding on access to these small/no-ELM regimes is not yet available. Whether these small/no-ELM regimes can be robustly achieved and compatible with steady-state operations is still uncertain in future fusion reactors. Further works including both experimental and numerical study of the small/no-ELM regimes are needed to gain a detailed physics understanding on these regimes and also the predictive capability towards future fusion reactors.

Acknowledgements The authors would like to thank all members in the EAST team. This work was supported by the National MCF Energy R&D Program of China under contract No. 2019YFE03030000 and National Natural Science Foundation of China under Grant No. U19A20113, No. 12005263, No. 11975275, No. 11905143, No. 12005257, No. 12105187 and Special Research Assistant Funding of CAS and China Postdoctoral Science Foundation No. 2020M671913. Numerical calculations were also performed on the ShenMa High Performance Computing Cluster in Institute of Plasma Physics, Chinese Academy of Sciences.

Data availability The data that support the findings of this study are available from the corresponding author upon reasonable request.

Declarations

Conflict of interest On behalf of all authors, the corresponding authors state that there is no conflict of interest.

Open Access This article is licensed under a Creative Commons Attribution 4.0 International License, which permits use, sharing, adaptation, distribution and reproduction in any medium or format, as long as you give appropriate credit to the original author(s) and the source, provide a link to the Creative Commons licence, and indicate if changes were made. The images or other third party material in this article are included in the article's Creative Commons licence, unless indicated otherwise in a credit line to the material. If material is not included in the article's Creative Commons licence and your intended use is not permitted by statutory regulation or exceeds the permitted use, you will need to obtain permission directly from the copyright holder. To view a copy of this licence, visit <http://creativecommons.org/licenses/by/4.0/>.

References


- N. Asakura et al., Investigations of impurity seeding and radiation control for long-pulse and high-density H-mode plasmas in JT-60U. *Nucl. Fusion* **49**, 115010 (2009)

- M.N.A. Beurskens et al., Pedestal and ELM response to impurity seeding in JET advanced scenario plasmas. *Nucl. Fusion* **48**, 095004 (2008)
- A. Bokshi et al., The response of toroidal drift modes to profile evolution: a model for small-ELMs in tokamak plasmas? *Plasma Phys. Control. Fusion* **58**, 075011 (2016)
- R. Chen et al., Experimental study on the magnetic coherent mode in the H-mode pedestal of EAST. *Nucl. Fusion* **58**, 112004 (2018)
- J.W. Connor et al., Magnetohydrodynamic stability of tokamak edge plasmas. *Phys. Plasmas* **5**, 2687 (1998)
- B. Debabrata et al., Stabilizing effect of resistivity towards ELM-free H-mode discharge in lithium-conditioned NSTX. *Nucl. Fusion* **57**, 076005 (2017)
- A. Diallo, First observation of ELM suppression without confinement degradation due to geodesic acoustic mode (GAM)-like mode triggered by boron powder injection. In: 28th IAEA Fusion Energy Conference (FEC 2020), Nice, France, (2021)
- D. Dickinson et al., Structure of micro-instabilities in tokamak plasmas: stiff transport or plasma eruptions? *Phys. Plasmas* **21**, 010702 (2014)
- G.F. Ding et al., Comparison of natural grassy ELM behavior in favourable/unfavourable Bt in EAST. *Plasma Sci. Technol.* **23**, 095105 (2021)
- E.J. Doyle et al., Chapter 2: Plasma confinement and transport. *Nucl. Fusion* **47**, S18 (2007)
- M.G. Dunne et al., Global performance enhancements via pedestal optimization on ASDEX Upgrade. *Plasma Phys. Control. Fusion* **59**, 025010 (2017)
- T. Eich et al., ELM divertor peak energy fluence scaling to ITER with data from JET, MAST and ASDEX upgrade. *Nucl. Mater. Energy* **12**, 84 (2017)
- X. Feng et al., I-mode investigation on the experimental advanced superconducting tokamak. *Nucl. Fusion* **59**, 096025 (2019)
- A. Fukuyama et al., Theory of improved confinement in high-beta tokamaks. *Plasma Phys. Control. Fusion* **36**, 1385 (1994)
- J. Garcia et al., New H-mode regimes with small ELMs and high thermal confinement in the Joint European Torus. *Phys. Plasmas* **29**, 032505 (2022)
- A.M. Garofalo et al., A fusion nuclear science facility for a fast-track path to DEMO. *Fusion Eng. Des.* **89**, 876 (2014)
- X. Gong et al., Integrated operation of steady-state long-pulse H-mode in experimental advanced superconducting tokamak. *Nucl. Fusion* **59**, 086030 (2019)
- M. Greenwald et al., Characterization of enhanced D alpha high-confinement modes in Alcator C-mod. *Phys. Plasmas* **6**, 1943–1949 (1999)
- G.F. Harrer et al., Parameter dependences of small edge localized modes (ELMs). *Nucl. Fusion* **58**, 112001 (2018)
- G.F. Harrer et al., Quasicontinuous exhaust scenario for a fusion reactor: the renaissance of small edge localized modes. *Phys. Rev. Lett.* **129**, 165001 (2022)
- J.S. Hu et al., New steady-state quiescent high-confinement plasma in an experimental advanced superconducting tokamak. *Phys. Rev. Lett.* **114**, 055001 (2015)
- K. Ibano et al., Estimation of suppressed erosion by vapor shielding at Be and W walls under transient loads. *Nucl. Fusion* **59**, 076001 (2019)
- ITER Organization, ITER Research Plan within the Staged Approach (Level III—Provisional Version), ITER Technical Report, ITR-18-003, (2018) <https://www.iter.org/technical-reports>
- Y. Kamada et al., Disappearance of giant ELMs and appearance of minute grassy ELMs in JT-60U high-triangularity discharges. *Plasma Phys. Control. Fusion* **42**, A247 (2000)
- K. Kamiya et al., High, recycling steady H-mode regime in the JFT-2M tokamak. *Plasma Phys. Control. Fusion* **46**, A157–A163 (2004)
- K. Kamiya et al., Edge localized modes: recent experimental findings and related issues. *Plasma Phys. Control. Fusion* **49**, S43 (2007)
- N. Klimov et al., Experimental study of PFCs erosion under ITER-like transient loads at plasma gun facility QSPA. *J. Nucl. Mater.* **390–391**, 721–726 (2009)
- B. Labit et al., Dependence on plasma shape and plasma fueling for small edge-localized mode regimes in TCV and ASDEX Upgrade. *Nucl. Fusion* **59**, 086020 (2019)
- Z.-Y. Li et al., Ideal MHD stability and characteristics of edge localized modes on CFETR. *Nucl. Fusion* **58**, 016018 (2018)
- K.D. Li et al., Divertor detachment with neon seeding in grassy-ELM H-mode in EAST. *Plasma Phys. Control. Fusion* **62**, 095025 (2020)

- Z.-Y. Li et al., Edge localized mode characteristics and divertor heat flux during stationary and transient phase for CFETR hybrid scenario. *Plasma Phys. Control. Fusion* **63**, 035006 (2021a)
- K.D. Li et al., Comparison of divertor behavior and plasma confinement between argon and neon seeding in EAST. *Nucl. Fusion* **61**, 066013 (2021b)
- Y. Liang et al., Magnetic topology changes induced by lower hybrid waves and their profound effect on edge-localized modes in the EAST tokamak. *Phys. Rev. Lett.* **110**, 235002 (2013)
- X. Lin et al., Physical mechanisms for the transition from type-III to large ELMs induced by impurity injection on EAST. *Phys. Lett. A* **431**, 127988 (2022)
- A. Loarte et al., ELM energy and particle losses and their extrapolation to burning plasma experiments. *J. Nucl. Mater.* **313–316**, 962–966 (2003a)
- A. Loarte et al., Characteristics of type I ELM energy and particle losses in existing devices and their extrapolation to ITER. *Plasma Phys. Control. Fusion* **45**, 1549 (2003b)
- R. Maingi et al., Observation of a high performance operating regime with small edge-localized modes in the National Spherical Torus Experiment. *Nucl. Fusion* **45**, 264 (2005)
- R. Maingi et al., Edge-localized-mode suppression through density-profile modification with lithium-wall coatings in the national spherical torus experiment. *Phys. Rev. Lett.* **103**, 075001 (2009)
- R. Maingi et al., Comparison of small ELM characteristics and regimes in Alcator C-Mod, MAST and NSTX. *Nucl. Fusion* **51**, 063036 (2011)
- D.K. Mansfield et al., First observations of ELM triggering by injected lithium granules in EAST. *Nucl. Fusion* **53**, 113023 (2013)
- S. Mordijck, Overview of density pedestal structure: role of fueling versus transport. *Nucl. Fusion* **60**, 082006 (2020)
- R. Nazikian et al., Grassy-ELM regime with edge resonant magnetic perturbations in fully noninductive plasmas in the DIII-D tokamak. *Nucl. Fusion* **58**, 106010 (2018)
- T.H. Osborne et al., Enhanced H-mode pedestals with lithium injection in DIII-D. *Nucl. Fusion* **55**, 063018 (2015)
- N. Oyama et al., Pedestal conditions for small ELM regimes in tokamaks. *Plasma Phys. Control. Fusion* **48**, A171 (2006)
- M. Romanelli et al., Modelling of plasma performance and transient density behavior in the H-mode access for ITER gas fuelled scenarios. *Nucl. Fusion* **55**, 093008 (2015)
- J. Roth et al., Recent analysis of key plasma wall interactions issues for ITER. *J. Nucl. Mater.* **390–391**, 1–9 (2009)
- G. Saibene et al., Characterization of small ELM experiments in highly shaped single null and quasi-double-null plasmas in JET. *Nucl. Fusion* **45**, 297 (2005)
- O. Sauter et al., Neoclassical conductivity and bootstrap current formulas for general axisymmetric equilibria and arbitrary collisionality regime. *Phys. Plasmas* **6**, 2834 (1999)
- P.A. Schneider et al., Observation of different phases during an ELM crash with the help of nitrogen seeding. *Plasma Phys. Control. Fusion* **56**, 025011 (2014)
- M. Shimada et al., Performance of ITER as a burning plasma experiment. *Nucl. Fusion* **44**, 350 (2004)
- J. Stober et al., Type II ELMy H modes on ASDEX upgrade with good confinement at high density. *Nucl. Fusion* **41**, 1123 (2001)
- J. Stober et al., Small ELM regimes with good confinement on JET and comparison to those on ASDEX Upgrade, Alcator C-mod and JT-60U. *Nucl. Fusion* **45**, 1213 (2005)
- Y. Sun et al., Nonlinear transition from mitigation to suppression of the edge localized mode with resonant magnetic perturbations in the EAST tokamak. *Phys. Rev. Lett.* **117**, 115001 (2016)
- Z. Sun et al., Suppression of edge localized modes with real-time boron injection using the tungsten divertor in EAST. *Nucl. Fusion* **61**, 014002 (2021)
- Y. Ueda et al., Baseline high heat flux and plasma facing materials for fusion. *Nucl. Fusion* **57**, 092006 (2017)
- E. Viezzer, Access and sustainment of naturally ELM-free and small-ELM regimes. *Nucl. Fusion* **58**, 115002 (2018)
- P. Vincenzi et al., Fuelling and density control for DEMO. *Nucl. Fusion* **55**, 113028 (2015)
- Y. Wan et al., Overview of the present progress and activities on the CFETR. *Nucl. Fusion* **57**, 102009 (2017)
- B.N. Wan et al., Recent advances in EAST physics experiments in support of steady-state operation for ITER and CFETR. *Nucl. Fusion* **59**, 112003 (2019)

- Y. Wan et al., Overview progress and future plan of EAST project, Proc. 21st IAEA Fusion Energy Conference 2006 <http://naweb.iaea.org/napc/physics/fec/fec2006/html/index.htm>
- H.Q. Wang et al., New edge coherent mode providing continuous transport in long-pulse H-mode plasmas. *Phys. Rev. Lett.* **112**, 185004 (2014)
- H.Q. Wang et al., Effects of low-Z and high-Z impurities on divertor detachment and plasma confinement. *Nucl. Mater. Energy* **12**, 942–947 (2017)
- Y.F. Wang et al., Grassy ELM regime at low pedestal collisionality in high-power tokamak plasma. *Nucl. Fusion* **61**, 016032 (2021)
- H.R. Wilson et al., Ideal magnetohydrodynamic stability of the tokamak high-confinement-mode edge region. *Phys. Plasmas* **6**, 1925 (1999)
- E. Wolfrum et al., Impact of wall materials and seeding gases on the pedestal and on core plasma performance. *Nucl. Mater. Energy* **12**, 18 (2017)
- K. Wu et al., The achievement of the Te, div feedback control by CD4 seeding on EAST. *Plasma Phys. Control. Fusion* **63**, 105004 (2021)
- T.Y. Xia et al., Divertor heat flux simulations in ELMy H-mode discharges of EAST. *Nucl. Fusion* **57**, 116016 (2017)
- G. S. Xu, Observation of Pressure-gradient-driven TAEs in the H-mode pedestal of the EAST Tokamak. In: 11th Westlake International Symposium on Energetic Particle Physics and Microturbulence in Magnetic Fusion, Hangzhou, China, (2017)
- G.S. Xu et al., Promising high-confinement regime for steady-state fusion. *Phys. Rev. Lett.* **122**, 255001 (2019)
- G.S. Xu et al., Divertor impurity seeding with a new feedback control scheme for maintaining good core confinement in grassy-ELM H-mode regime with tungsten monoblock divertor in EAST. *Nucl. Fusion* **60**, 086001 (2020)
- G. S. Xu, ELM suppression sustained by an edge low-n mode excited by divertor impurity seeding in detached H-mode plasmas in EAST. In: 28th IAEA Fusion Energy Conference (FEC 2020), Nice, France (2021)
- Q.Q. Yang et al., Stationary high-performance grassy ELM regime in EAST. *Nucl. Fusion* **60**, 076012 (2020)
- Y. Ye et al., A stationary long-pulse ELM-absent H-mode regime in EAST. *Nucl. Fusion* **57**, 086041 (2017)
- Y. Ye et al., Experimental study on low recycling no-ELM high confinement mode in EAST. *Nucl. Fusion* **59**, 086044 (2019)
- Y. Ye et al., Sustained edge-localized-modes suppression and radiative divertor with an impurity-driven instability in tokamak plasmas. *Nucl. Fusion* **61**, 116032 (2021)
- H. Zhang et al., Observation of a fully non-inductive H-mode regime dominated by the sporadic-small edge-localized modes in EAST with a tungsten divertor. *Plasma Phys. Control. Fusion* **61**, 085006 (2019)
- B. Zhang et al., H-mode operation in helium plasma with tungsten divertor and low input torque in EAST. *Nucl. Fusion* **60**, 092001 (2020)
- C. Zhao et al., Gyrokinetic simulation of dissipative trapped electron mode in tokamak edge. *Phys. Plasmas* **24**, 052509 (2017)
- A. Zhitlukhin et al., Effects of ELMs on ITER divertor armour materials. *J. Nucl. Mater.* **363–365**, 301–307 (2007)
- W.L. Zhong et al., Impact of impurity mixture gas seeded by supersonic molecular beam injection on edge-localized modes in the HL-2A tokamak. *Nucl. Fusion* **59**, 076033 (2019)
- G. Zhuang et al., Progress of the CFETR design. *Nucl. Fusion* **59**, 112010 (2019)
- X. L. Zou et al., IAEA Fusion Energy Conference (FEC 2012), San Diego, USA, PD/P8-08 <http://naweb.iaea.org/napc/physics/FEC/FEC2012/html/fec12.htm>

Authors and Affiliations

G. S. Xu¹ · Y. F. Wang¹ · Q. Q. Yang¹ · X. Lin¹  · R. Chen¹ · Y. Ye² · H. Lan^{1,3,4} · N. Yan¹

✉ X. Lin
linxin@ipp.ac.cn

¹ Institute of Plasma Physics, Hefei Institutes of Physical Science, Chinese Academy of Sciences, Hefei 230031, China

² Institute of Energy, Hefei Comprehensive National Science Center, Hefei 230031, China

³ College of Physics and Optoelectronic Engineering, Shenzhen University, Shenzhen 518060, China

⁴ Advanced Energy Research Center, Shenzhen University, Shenzhen 518060, China